PAPER

High field vortex phase diagram of Fe(Se, Te) thin films

IOP Publishing Superconductor Science and Technology
Supercond. Sci. Technol. **27** (2014) 044007 (6pp) doi:10.1088/0953-2048/27/4/044007

High field vortex phase diagram of Fe(Se, Te) thin films

E Bellingeri[1], S Kawale[1,2], F Caglieris[1,2], V Braccini[1], G Lamura[1], L Pellegrino[1], A Sala[1,2], M Putti[1,2], C Ferdeghini[1], A Jost[3], U Zeitler[3], C Tarantini[4] and J Jaroszynski[4]

[1] CNR–SPIN Genova, Corso Perrone 24, I-16152 Genova, Italy
[2] Physics Department, University of Genova, Via Dodecaneso 33, I-16146 Genova, Italy
[3] High Field Magnet Laboratory, Institute for Molecules and Materials, Radboud University Nijmegen, 6525 ED Nijmegen, The Netherlands
[4] Applied Superconductivity Center, National High Magnetic Field Laboratory, Florida State University, 2031 E Paul Dirac Drive, Tallahassee, FL 32310, USA

E-mail: emilio.bellingeri@spin.cnr.it

Received 13 September 2013, revised 4 November 2013
Accepted for publication 9 November 2013
Published 18 March 2014

Abstract
We report on the (H, T) vortex phase diagram up to 35 T of Fe(Se, Te) thin films deposited on CaF_2 substrates as determined by resistivity, Nernst effect and critical current measurements. We found the presence of a large region where the vortex is firmly pinned, allowing the adoption of chalcogenides for low temperature but extremely high magnetic field applications. The fact that high critical current density values—larger than 1 MA cm^{-2} in self-field and liquid helium—are reached together with a very weak dependence on the magnetic field and a complete isotropy, joined with the very high rigidity of the vortex lattice at very high field, makes the Fe(Se, Te) phase very promising for low temperature ($\leqslant$4.2 K) and high field ($\geqslant$25 T) applications.

Keywords: chalcogenides, thin films, vortex phase diagram, Nernst effect, transport properties

(Some figures may appear in colour only in the online journal)

1. Introduction

Despite their relatively low critical temperature (T_c) values, typically below 15 K, chalcogenides are an interesting subclass of iron-based superconductors. In fact, in FeSe, T_c can reach 37 K under a pressure of 7 GPa [1], and it can be increased up to 21 K in Fe(Se, Te) thin films due to the residual strain [2]. They also have the simplest structure among the iron-based superconductors and exhibit lower anisotropies, with comparable $H_{c2}(0)$ well above 50 T [3]. Furthermore, high irreversibility line H_{irr} very close to the upper critical field H_{c2} makes this class of superconductors particularly appealing for high-field–low temperature applications, where the major limiting factor is the critical current density J_c.

Although the high-T_c cuprates currently hold the records of J_c, H_{c2} and H_{irr} values among all superconductors, there are quite a few obstacles to their practical application. The extremely high anisotropies, up to several hundreds, and the rapid decrease of J_c upon the grain boundary misorientation make it very difficult to obtain superconducting tapes or wires with the best possible J_c. Their brittle texture as well as the high production and raw material costs hold back their application. Currently, superconductors for high field application are still based on Nb_3Sn, a low T_c superconductor that allows fields in excess of 20 T to be achieved at 4.2 K.

Recently we reported that epitaxial Fe(Se, Te) thin films deposited on CaF_2(001), which reach critical current density larger than 1 MA cm^{-2} in self-field and approach 0.5 MA cm^{-2} at 9 T, exhibit very weak field and angular dependences [4]. Superior high field performance up to 30 T with $J_c > 1$ MA cm^{-2} in self-field in epitaxially grown iron-chalcogenide thin films with a CeO_2 buffer layer deposited on RABiTS substrates has been demonstrated [5], disclosing the future possibility of producing long length

conductors. We argue that iron superconductors may be a more competitive candidate to replace Nb-based superconductors for high field applications at liquid helium temperatures.

In this framework a deep analysis of the superconducting vortex phase diagram is necessary in order to reach a full understanding and control of the high current transport in these materials. Resistivity measurements under high magnetic field are a simple but powerful tool to investigate vortex line dynamics, allowing identification of H_{c2}, H_{irr} and the activation energy. The Nernst and Ettinghausen effects are very sensitive techniques to detect the vortex motion as they can detect the start of the vortex lattice melting and also the possible existence of vortex-like excitations above T_c [6–8].

In this paper we report on the (H, T) vortex phase diagram up to 35 T as determined by resistivity, Nernst effect and critical current measurements of Fe(Se, Te) thin films deposited on CaF_2 substrates. We found the presence of a large region where the vortex is firmly pinned, allowing the adoption of this kind of material for low temperature but extremely high magnetic field applications.

2. Experimental details

The films were grown by pulsed laser deposition (PLD) in an ultra-high vacuum system starting from an $FeSe_{0.5}Te_{0.5}$ target prepared by direct synthesis from high purity materials (Fe 99.9 + %, Se 99.9% and Te 99.999%) by a two-step procedure. (001) oriented CaF_2 single crystals were used as substrates: the substrates were glued by silver paint onto a stainless steel sample holder placed on a resistive heater. The films were deposited under high vacuum conditions at a residual gas pressure of 5×10^{-9} mbar at the deposition temperature. The quality of the growth was monitored *in situ* by reflection high energy electron diffraction (RHEED). The deposition conditions were optimized as reported in previous papers [9, 10] but, differently from the cited paper, we used a Nd:YAG laser at 1024 nm in place of the KrF at 248 nm wavelength. The use of the 1024 nm wavelength allowed a better reproducibility of the depositions and a more controlled target consumption. The other deposition parameters were 550 °C as the deposition temperature, 3 Hz as the laser repetition rate, 0.5 J cm^{-2} (2 mm^2 spot size) as the laser fluency and 5 cm as the target–substrate distance. XRD analysis confirmed the high quality and purity of the films, and ϕ scans indicated that the film grows rotated by 45° with respect to the a axis of 5.4620 Å due to the good matching with half the diagonal $a/\sqrt{2} = 3.862$ Å [11].

We previously discussed how the morphology is affected by the deposition rate [12]: films presented here are approximately grown in the high rate conditions which result in a strained film with higher T_c as already shown in [2], where we demonstrated that the growth induces planar strain, which is biaxial and 2% in magnitude, and it yields a T_c enhancement up to 21 K.

Hall bar shaped microbridges of 10, 20 and 50 μm width and 65 and 1000 μm distance between the voltage contacts were realized by conventional photolithography and water cooled Ar ion milling etching. The T_c measured on the different filaments is the same, showing an onset of 20.5 K and a $T_{c,0}$ value of 19 K.

Resistivity was measured up to 35 T at the NHMFL in Tallahassee, FL by the four probe technique in DC field with the sample oriented parallel and perpendicular to the magnetic field. The measurements were performed in maximum Lorentz force configuration, ramping temperature at constant applied field.

Magnetothermoelectric effect was measured up to 30 T at the High Field Magnet Laboratory in Nijmegen, The Netherlands. During the measurements the magnetic field was kept fixed and the temperature slowly swept. A thermal gradient was induced in the sample by applying small heat pulses to one side of the film by a resistive heater and the temperatures were measured by two RuO_x thermometers glued on the back of the substrate. In order to measure a significant effect a quite large gradient of the order of 1–1.5 K was necessary, resulting in quite broad curves. The magnetothermal effect was obtained as the difference of the voltage measured switching the heater on and off, and finally the Nernst effect was obtained by taking the semi difference of the voltage signal of a positive and negative magnetic field temperature sweep.

Transport critical current measurements of the microbridges as a function of temperature, magnetic field and angle with respect to the field were performed up to 9 T in a Physical Properties Measuring System (PPMS) by Quantum Design operating with a sample rotator. Current versus voltage characteristics (I–V) were acquired sweeping the current from zero with exponentially increasing steps, with the aim of avoiding heating problems. The critical current value is defined with the standard 1 μV cm^{-1} criterion.

3. Results and discussion

Figures 1(a) and (b) show the resistive transition of the patterned film under magnetic field up to 35 T applied parallel and perpendicular to the ab planes respectively. A T_c onset of 20.5 K and a quite narrow transition with a $T_{c,0}$ of 19 K are observed in zero field. The superconductivity appears to be quite robust in this sample, being a zero resistance state reached above 12 K and 9 K when a magnetic field of 35 T is applied parallel and perpendicular to the ab planes respectively. H_{c2} and H_{irr} values were estimated by the usual criterion of 90% and 10% of normal state resistivity respectively. The results are shown in figure 2, where $H_{c2}(T)$ with downward curvatures for both field orientations and very steep slopes at T_c are observed. The fit of the data both on the 0–3 T and 0–5 T ranges gives a slope of 100 T K^{-1} for the ab direction and of about 30 T K^{-1} in the c direction. Such high values are in agreement with previous reported values measured on our strained film deposited on $LaAlO_3$ and explained in terms of an extreme Pauli-limited $H_{c2}(T)$, indicative of the Fulde–Ferrell–Larkin–Ovchinnikov (FFLO) state [3].

The H_{c2} curves obtained for the two orientations are quite similar and only a relatively small anisotropy is observed: the ratio $H_{c2}^{\|ab}/H_{c2}^{\|c}$ at 16 K is only 1.2. The resistive transitions are quite narrow even in high magnetic field, so the irreversibility lines are quite close to the upper critical field. H_{irr} only shows

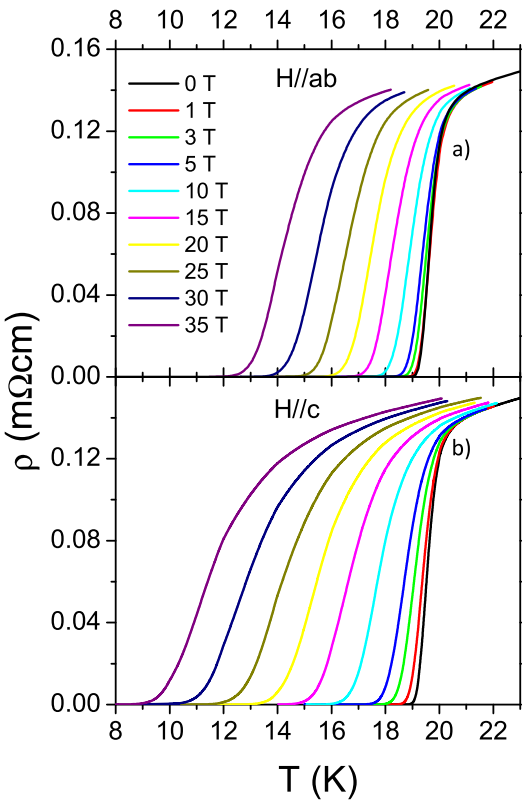

Figure 1. Resistive transitions in magnetic field up to 35 T, applied parallel (a) and perpendicular (b) to the *ab* plane.

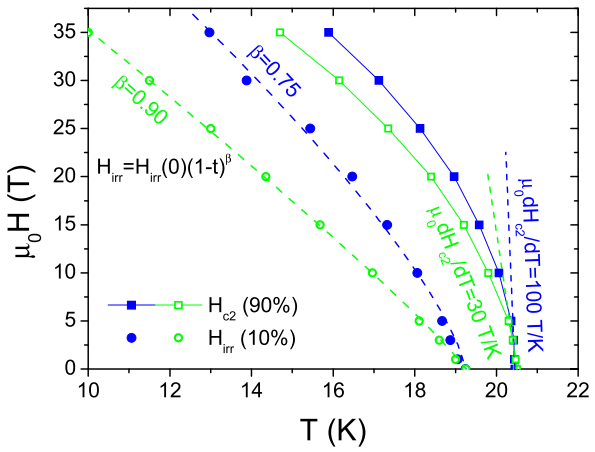

Figure 2. Upper critical field and irreversibility line as derived from resistive transitions in parallel and perpendicular directions. The slope of H_{c2} close to T_c is also shown. H_{irr} are fitted by power law.

a slightly more pronounced anisotropy: the ratio $H_{irr}^{\|ab}/H_{irr}^{\|c}$ at 16 K is about 1.6. Also the behaviour is slightly different in the two orientations: $H_{irr}^{\|ab}$ shows a downward curvature, mimicking the H_{c2} shape, whereas $H_{irr}^{\|c}$ is almost linear up to the highest applied field.

In the mixed dissipative state the flux motion is described by the thermal activated flux flow, where the resistivity is described by [13, 14]

$$\rho = \frac{2\nu_0 L\mu_0 H}{J} e^{-J_{c0}\mu_0 HV/T} \sinh\left(\frac{J\mu_0 HV}{T}\right)$$

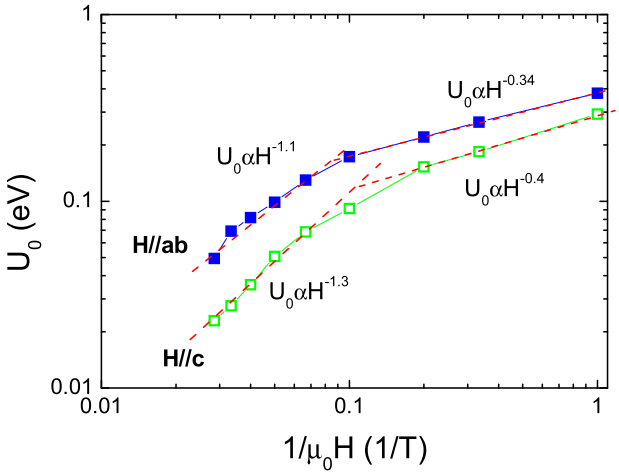

Figure 3. Vortex motion activation energy as a function of the inverse of the field in parallel (blue full symbols) and perpendicular (green hollow symbols) configurations as extracted from the Arrhenius plot.

where ν_0 is an attempt hopping frequency, L the hopping distance, J the applied current density, J_{c0} the critical current in absence of flux creep, and V the volume of the hopping vortex bundle. Usually resistivity measurements are performed at very low applied J and within a further simplifying hypothesis introduced for HTSC which can be considered valid also for the case of an iron-based superconductor ([15] and references therein): the formula can therefore be written as the simpler Arrhenius relationship

$$\rho = \rho_0(H)e^{-U_0(H)/K_B T}.$$

The Arrhenius plot ($\ln\rho$ versus $1/T$) of the resistivity data of figure 1 shows a quite wide linear region indicating the sustainability of the above cited approximation. The U_0 values estimated by the linear fit are plotted as a function of the inverse of the applied magnetic field in figure 3: the $U_0(H)$ values in the two orientations have a different magnitude but a similar trend in magnetic field. The data are usually fitted by a power law $U_0 \propto H^{-\alpha}$ but, as shown in the figure, a single exponent is not sufficient to fit the data in the whole magnetic field range. Up to about 10 T a weak dependence on the magnetic field is observed in both field directions, being the data well fitted by $\alpha = 0.34$ and 0.4 with the field parallel and perpendicular to the *ab* planes, respectively, whereas a more pronounced field dependence is observed for higher field with $\alpha = 1.1$ and 1.3 in the two directions. More generally, a crossover from individual pinning regime ($\alpha < 0.5$) to interacting vortex regime ($\alpha > 0.8$–1) is always observed in the literature data on U_0 in an iron-based superconductor even if the crossover from one regime to another is usually observed at lower field [16–19]. This finding suggests that in our films on CaF_2 the individual pinning regime, corresponding to the lower α value, is active up to almost 10 T, which means that the relevant pinning energy is larger than the vortex–vortex interaction.

J_c measured as a function of the magnetic field (only up to 9 T) is reported at the temperatures of 4, 9.5 and 15 K in figure 4(a) for the field applied parallel and perpendicular

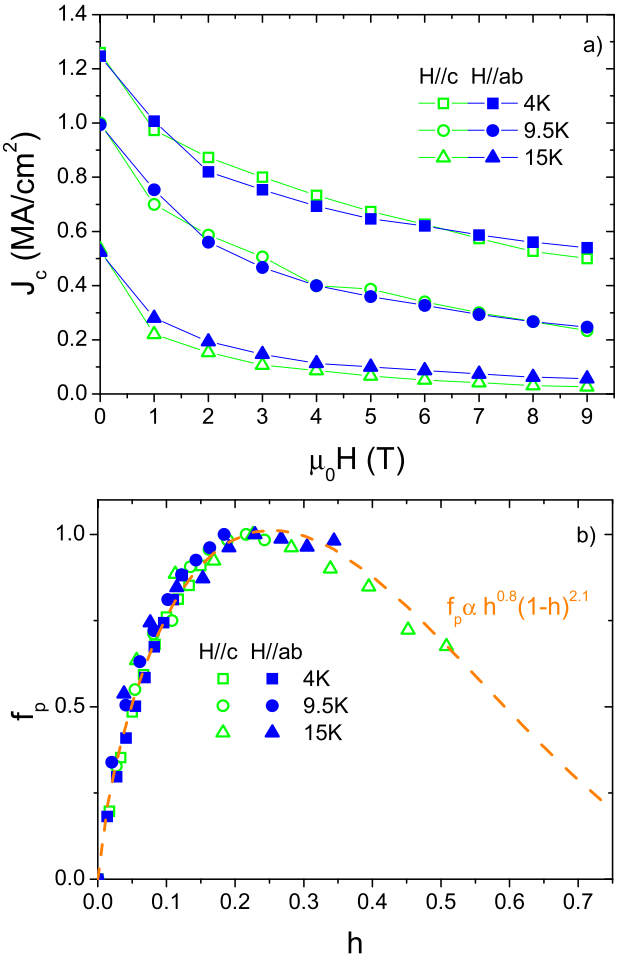

Figure 4. (a) Critical current density as a function of magnetic field at selected temperatures, and (b) the relative normalized pinning force as a function of the reduced magnetic field $H/H_{\rm irr}$. The curves are fitted by the Dew-Hughes relation.

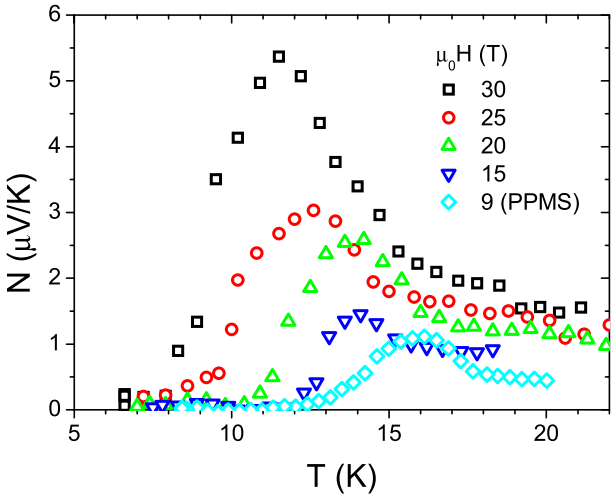

Figure 5. Nernst signal as a function of the temperature at different magnetic fields.

Table 1. $H_{\rm irr}$ values obtained by data in figure 2. Italic values are extrapolation by the power law fit of the data.

$\mu_0 H_{\rm irr}$ (T)	15 K	9.5 K	4 K
$H \parallel ab$	26	*49*	*55*
$H \parallel c$	18	*37*	*68*

to the *ab* plane [4]. In self-field J_c is above 1 MA cm^{-2} at 4 K, which is among the highest values ever observed in the 11 phase by direct transport measurements: J_c (0 T, 4.2 K) = 1 MA cm^{-2} was also reported by Si *et al* [5] on $FeSe_{1-x}Te_x$ thin films realized on CeO-buffered RABiTs technical substrates. Slightly lower values were obtained by Iida *et al* [20] on $FeSe_{1-x}Te_x$ thin films realized on Fe-buffered MgO substrates and Si *et al* [21] for films deposited on $LaAlO_3$.

As expected from the steep irreversibility line presented in figure 2, remarkably high critical current density values are sustained increasing both the temperature and the magnetic field: at $T = 15$ K, which is 80% of $T_{c,0}$, we still measured J_c (0 T, $t = 0.8$) = 0.4 MA cm^{-2}. Analysing the behaviour of J_c with the field, we notice that the field dependence is very weak especially at low temperatures: J_c in fact halves its value increasing the magnetic field from 0 to 9 T; moreover, J_c is almost isotropic at 4 and 9.5 K, where the J_c values measured with the field parallel and perpendicular to the *ab* planes perfectly match.

The $H_{\rm irr}$ lines in figure 2 can be well fitted by a power relationship $H_{\rm irr}(t) = H_{\rm irr}(0)(1-t)^{\beta}$ where t is the reduced temperature $t = T/T$ ($H_{\rm irr} = 0$) and thus it is possible to confidently extrapolate the $H_{\rm irr}$ values at 9.5 and 4 K (see table 1). Using these values to scale H we can calculate the pinning force $F_p = \mu_0 H \times J_c$ and plot its normalized value $f_p = F_p/F_{p\max}$ as a function of $h = H/H_{\rm irr}$.

As can be seen in figure 4(b), data for all temperatures and both directions lay approximately on a single line. This indicates that the pinning mechanism is independent of the temperature and field direction. Following Dew-Hughes [22] the data can be fitted by $f_p \propto h^p(1-h)^q$ with $p = 0.8$ and $q = 2.1$. These parameters give a maximum of the curves at $h_{\max} = 0.28$ that is intermediate between the values of $h_{\max} = 0.2$ and $h_{\max} = 0.33$ expected for surface and point-defect pinning respectively. However, the values of $p = 0.8$ and $q = 2.1$ are quite close to the expected $p = 1$ and $q = 2$ for the case of normal-core point pinning. Thus $h_{\max} \sim 0.28$ can be understood in terms of δl type pinning with a mixture of the surface and the point core pinning of the normal centres, with the different range of the pinning interactions. This is in agreement with our TEM observation in the same samples of local lattice displacements with the size of a flux core that can act well as pinning centre [4]. These results are in full agreement with the values reported by Si *et al* [5] indicating a similar origin of the pinning mechanism.

Further information on the vortex state can be extracted from the magnetothermoelectric effect. In particular in the mixed state the vortices under the thermal force move in the direction parallel to the temperature gradient ∇T, transfer the magnetic flux, and in this way induce the transverse Nernst voltage [23].

At very low temperatures and high field vortex matter ideally organizes itself into a vortex lattice and the Nernst effect is generally negligible: this can be qualitatively understood as a result of rigidity of the lattice. Increasing the temperature

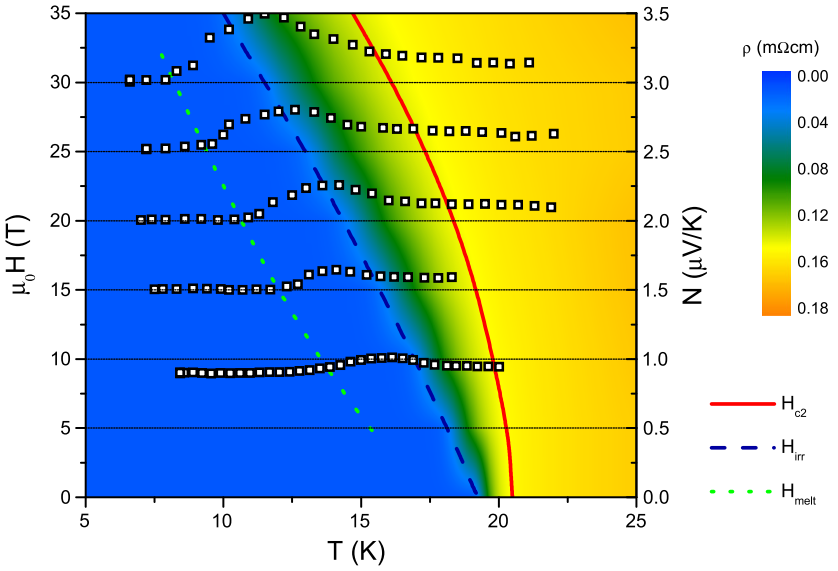

Figure 6. Fe(Se, Te) vortex phase diagram combined from resistivity (2D plot) H_{c2} and H_{irr} (left scale) and offset (see text) Nernst effect (right scale). All quantities are measured with the magnetic field applied perpendicular to the *ab* planes.

the long range order of the lattice is lost but the vortex remains pinned due to the unavoidable presence of disorder, and vortices form a Bragg glass. Also in this case the Nernst signal is very small. A large Nernst voltage peak appears only when this glass state melts and the vortex can move. The measured Nernst voltage on our Hall bar patterned film is shown in figure 5: the region of vortex motion is clearly identified by the presence of a peak that shifts to lower temperature with increasing magnetic field and its amplitude steadily increases up to the highest measured field of 30 T. These results are in agreement with previously reported Nernst effect measurements reported on Fe(Se, Te) single crystal [24, 25].

In order to summarize the information on the vortex state obtained by means of different measurements, we report in figure 6 the resistivity of the film plotted in greyscale (colour online) in the 2D plot as function of temperature and magnetic field in the horizontal and vertical axes respectively.

The solid and dashed lines represent the $H_{c2}(T)$ and $H_{irr}(T)$ respectively as obtained from the resistivity (respectively from 90% and 10% of the resistive transition). The Nernst voltage signal is also plotted on the same figure: an offset has been introduced in such a way that the zero of each curve lies at the correspondent magnetic field (i.e. the 0 of the curve measured at 15 T lies on a line at 15 T). All the quantities reported in figure 6 were measured with the magnetic field applied perpendicular to the *ab* planes. As expected, the maxima of the Nernst effect are in the region of high vortex flow where the resistivity starts to rise, thus well matching with the $H_{irr}(T)$ line (defined as 10% of normal state resistance). The Nernst effect, differently from what happens in many HTSCs, reaches its normal state value approximately at the $H_{c2}(T)$ line, indicating that vortices do not survive significantly above T_c, as the thermodynamic fluctuations are negligible in this material. The onset of the Nernst signal is evidenced in the graph as the $H_{melt}(T)$ line (dotted): this line—fairly steep and with an upward curvature, up to the highest field measured—represents the separation between a region where the vortices, in a regular lattice or in a glassy state, form a rigid and pinned structure, and a region where they start to move and dissipation occurs and probes the true irreversibility field, giving a more reliable and physical estimation of it than the 10% of the resistive transition—which lies slightly higher and is only one of the possible definitions for H_{irr}.

4. Conclusions

In summary we can conclude that the vortex phase diagram of these films is simpler than that observed in the case of HTSC materials. In particular we showed that the vortex motion can be well described by a single $U_0(H)$ value in almost the whole temperature range and that $U_0(H)$ has the same behaviour in both of the orientations of the magnetic field with a change from individual to collective pinning at around 10 T. The good scaling of the pinning force from 4 to 15 K for both of the directions of the field appears to suggest that the pinning mechanism is independent of the temperature and field direction. The fitting parameters indicate that a point-defect core pinning mechanism is involved which can be identified in the lattice defect we observed through TEM analysis. Noticeably, in this regime, the global pinning force is the product of the individual force of the defect times the pinning centre density. This means that the J_c of chalcogenides may still be enhanced by the introduction of more defects acting as pinning centres.

These results are very interesting from an applicative point of view: indeed, the fact that very high critical currents are sustained up to 30 T as reported in [5], joined with the very high rigidity of the vortex lattice at very high field, as shown in this work, makes the Fe(Se, Te) phase very promising for low temperature ($\leq$4.2 K) and high field ($\geq$25 T) applications.

Acknowledgments

This work has been partially supported by FP7 European project SUPER-IRON (No. 283204) and EuroMagNET II (No. 228043). A portion of this work was performed at the National High Magnetic Field Laboratory, which is supported by National Science Foundation Cooperative Agreement No. DMR-1157490, the State of Florida, and the US Department of Energy.

References

[1] Margadonna S *et al* 2009 *Phys. Rev.* B **80** 064506
[2] Bellingeri E, Pallecchi I, Buzio R, Gerbi A, Marré D, Cimberle M R, Tropeano M, Putti M, Palenzona A and Ferdeghini C 2010 *Appl. Phys. Lett.* **96** 102512
[3] Tarantini C, Gurevich A, Jaroszynski J, Balakirev F, Bellingeri E, Pallecchi I, Ferdeghini C, Shen B, Wen H H and Larbalestier D C 2011 *Phys. Rev.* B **84** 184522
[4] Braccini V *et al* 2013 *Appl. Phys. Lett.* **103** 172601
[5] Si W *et al* 2013 *Nature Commun.* **4** 1347
[6] Wang Y, Ong N P, Xu Z A, Kakeshita T, Uchida S, Bonn D A, Liang R and Hardy W N 2002 *Phys. Rev. Lett.* **88** 257003
[7] Xu Z A, Ong N P, Wang Y, Kageshita T and Uchida S 2000 *Nature* **406** 486
[8] Wang Y, Xu Z A, Kakeshita T, Uchida S, Ono S, Ando Y and Ong N P 2001 *Phys. Rev.* B **64** 224519
[9] Bellingeri E *et al* 2009 *Supercond. Sci. Technol.* **22** 105007
[10] Bellingeri E *et al* 2012 *Supercond. Sci. Technol.* **25** 084022
[11] Kawale S, Bellingeri E, Braccini V, Pallecchi I, Putti M, Grimaldi G, Leo A, Guarino A, Nigro A and Ferdeghini C 2013 *IEEE Trans. Appl. Supercond.* **23** 7500704
[12] Gerbi A, Buzio R, Bellingeri E, Kawale S, Marrè D, Siri A S, Palenzona A and Ferdeghini C 2012 *Supercond. Sci. Technol.* **25** 012001
[13] Blatter G, Feigelman M V, Geshkenbein V B, Larkin A I and Vinokur V M 1994 *Rev. Mod. Phys.* **66** 1125
[14] Palstra T T M, Batlogg B, van Dover R B, Schneemeyer I F and Waszczak J V 1990 *Phys. Rev.* B **41** 6621
[15] Lei H *et al* 2012 *Sci. Technol. Adv. Mater.* **13** 054305
[16] Shahbazi M, Wang X L, Shekhar C, Srivastava O N, Lin Z W, Zhu J G and Dou S X 2011 *J. Appl. Phys.* **109** 07E162
[17] Jaroszynski J *et al* 2008 *Phys. Rev.* B **78** 174523
[18] Ghorbani S R, Wang X L, Shabazi M, Dou S X, Choi K Y and Lin C T 2011 arXiv:1109.3837
Lei H and Petrovic C 2011 arXiv:1110.5316
[19] Vinod K, Sharma S, Satya A T, Sundar C S and Bharathi A 2011 arXiv:1107.4170
[20] Iida K, Hänisch J, Schulze M, Aswartham S, Wurmehl S, Büchner B, Schultz L and Holzapfel B 2011 *Appl. Phys. Lett.* **99** 202503
[21] Si W, Zhou J, Jie Q, Dimitrov I, Solovyov V, Johnson P D, Jaroszynski J, Matias V, Sheehan C and Li Q 2011 *Appl. Phys. Lett.* **98** 262509
[22] Dew-Hughes D 1974 *Phil. Mag.* **30** 293
[23] Tinh B D and Rosenstein B 2009 *Phys. Rev.* B **79** 024518
[24] Pourret A, Malone L, Antunes A B, Yadav C S, Paulose P L, Fauque B and Behnia K 2011 *Phys. Rev.* B **83** 020504(R)
[25] Matusiak M, Pomjakushina E and Conder K 2012 *Physica* C **483** 21